Monte Carlo experiments for uncertainty investigation of glacier melt discharge predictions through surface energy balance analysis

FREDDY SORIA & SO KAZAMA

Civil Engineering Department, Tohoku University, Aoba Aramaki 6-6-06, PO Box 980-0871, Sendai, Japan

soria@kaigan.civil.tohoku.ac.jp

Abstract The spatial representativeness of point records is a concern in glacier discharge predictions. A Monte Carlo-based global sensitivity approach is used to investigate the predictive uncertainty in the net radiation (*Rn*) as the major component driving glacier melt in the Bolivian Andes. The *Rn* is inferred through the Surface and Energy Balance Algorithm, calibrated with point dry-season records monitored on a glacier's ablation area. High uncertainties are expected in the vicinity of the monitoring station (surface albedo (α) between 0.81 and 0.79, specific melt discharge (SMD) between 72 and 88 L s^{-1} km^{-2}); smaller uncertainties are expected on the glacier boundaries (α between 0.10 and 0.08, SMD between 128 and 143 L s^{-1} km^{-2}). Thus, with the incoming long wave radiation ($R_L\downarrow$) as the most sensitive model parameter, the spatial variability in α determines the spatial variability in the SMD predictive uncertainties.

Key words tropical Andes; sensitivity analysis; remote sensing

INTRODUCTION

The spatial representativeness of point records that arises from the complexity observed in natural systems, is a concern to mathematical modellers. In watershed numerical modelling (as a valid example), the classical "calibration" as a means to assure the adequacy of a given model has long been brought into question by several hydrological publications. These publications established our limitations in representing complex natural systems (e.g. Beven, 1993; Wagener *et al.*, 2004), emphasizing the need for the uncertainty reduction in predictions to be a primary aim. Thus, similar to watershed hydrology, the investigation of predictive uncertainty is a demanding topic in the prediction of glacier-melt discharge in remote areas, due to limited knowledge of the spatial distribution of surface processes resulting from the low spatial density of ground observations.

Our aim in this study is to investigate the uncertainty in the spatial representativeness of point data recorded on a glacier in the tropical Andes, through a sensitivity analysis approach inspired by the equifinality concept. The equifinality idea suggests that, given current levels of knowledge and measurement technologies, rather than a unique representation of a given system, the existence of a universe of behavioural models is likely. Beven (1993) formally introduces the equifinality idea in the hydrological literature. It became an inspiration for Wagener *et al.* (2004), who among others provide the basis for Tang *et al.* (2007) and Soria & Kazama (2011), whose ideas are applied in this study. The approach includes the application of remote sensing techniques as a tool to infer the spatial distribution of surface energy balance processes on glacial formations.

STUDY AREA AND DATA

The investigation is on the Zongo glacier in the Cordillera Real, situated in the tropical Andes in Bolivia. From a water resources engineering perspective, the melt from the ice caps of the Cordillera Real are worth studying because they provide freshwater for nearby ecosystems and for neighbouring urban settlements, La Paz and El Alto (approximate population of 1 000 000 people). The Zongo glacier (approx. 2 km^2 of ice cover, horizontal view) is a unique source of information for the study of tropical glaciers in the Andes of Bolivia.

The surface energy balance is investigated using point meteorological observations acquired on 26 July 2005 (at 5050 m a.m.s.l.) on the ablation zone of the Zongo glacier. The spatial distribution of the energy balance is inferred from the processing of a Landsat ETM+ 30-m horizontal resolution scene. The meteorological data are provided by the GLACIOCLIM (Les GLACIers, un Observatoire du CLIMat), and the Landsat scene was obtained from the US Geological Service (USGS) Earth Resources Observation and Science (EROS). The Landsat scene was acquired during the dry season (in the austral winter, 26 July 2005) at 10:30 h (local time). This scene was selected considering the small discrepancy with ground observations as observed in Soria & Kazama (2010). The calibration of the Landsat scene was carried out with the procedure suggested in Chander *et al*. (2009). The glacier-covered area was calculated from false colour composites (as in Soria & Kazama, 2009). The topographic information at 90-m horizontal resolution is from the Shuttle Radar Topography Mission Digital Elevation Model (SRTM DEM).

METHODS

The net radiation is assumed to be the major source of energy for glacier melt in the Cordillera Real. The instantaneous net radiation at the Landsat sensor acquisition time, *Rn*, is estimated through the Surface Energy Balance algorithm SEBAL (Bastiaanssen, 2000). The *Rn* is calibrated with the GLACIOCLIM point data. The uncertainty analysis is carried through a Monte Carlo variance-based global sensitivity analysis (Chan *et al.*, 2000).

Energy balance equation and simplifications

The energy available for glacier melt Q_M in W m^{-2} is investigated through equation (1), and the melt depth is calculated with equation (2) (Paterson, 1999):

$$Q_M = Rs + R_{L,n} + Q_H + Q_{LE} + Q_G + Q_P \quad (1)$$

$$M = \frac{Q_M \cdot \Delta t}{D_W \cdot \lambda_f} \quad (2)$$

In equation (1), *R*s is the net shortwave radiation, $R_{L,n}$ is the net longwave radiation, Q_H is the turbulent sensible heat, Q_{LE} is the turbulent latent heat flux, Q_G is the conductive-energy flux in the snow/ice or subsurface flux, and Q_P is the heat flux supplied by precipitation (Paterson, 1999). In equation (2), *M* (in m) is the melt depth for a time interval Δt due to Q_M in W m^{-2}, the density of water D_W is 1000 kg m^{-3}, and the latent heat of fusion of ice λ_f is 0.334 10^3 kJ kg^{-1}.

We assume that the calculations of Q_M are well represented by the net radiation *Rn* (i.e. the sum of *Rs* and $R_{L,n}$). The points below, (a) to (c), discuss such an assumption.

(a) The *Rs* and the incoming longwave radiation $R_L\downarrow$ are the most relevant sources of energy and can not be neglected. The *Rs* controls the variability of the energy balance during the melt season (which coincides with the glacier accumulation and the glacier ablation seasons), whereas the $R_L\downarrow$ is the main energy source for melting (Wagnon *et al.*, 1999).

(b) The turbulent fluxes Q_H and Q_{LE} tend to cancel each other during the melt season (the wet season) (Sicart *et al.*, 2008). This observation suggests that Q_H and Q_{LE} can be neglected for analysis conducted during the melt season. For the winter season (the dry season), the relevance of Q_H and the Q_{LE} is high due to the dry air at high elevations. However, for our analysis we assume that such error may not be large, given that average daily melt discharge rates during winter are notoriously low in comparison to melt season discharge rates (e.g. in the year 1999–2000, daily melt discharge in winter was about 10% of the peak melt discharge in the melt season (Sicart *et al.*, 2007).

(c) The Q_P is negligible because precipitation on the glacier always falls as snow (Wagnon *et al.*, 1999). The Q_G is negligible because it is excessively small in melt season; compared to *Rn* and turbulent fluxes, the Q_G is also small in winter (Wagnon *et al.*, 2009).

Other assumptions for glacier melt estimations

The equilibrium line is at approx. 5250 m a.m.s.l. (Sicart *et al.*, 2007). We assume that the runoff limit is at some distance above the equilibrium line (Rick, 2008). In the ablation zone, it is assumed that all melt contributes to runoff (Rick, 2008). In the accumulation zone, it is assumed that some melt is retained by refreezing of the percolated melt (Rick, 2008). We assume that Q_M is effective on the glacier portion below 5300 m a.m.s.l.. Above 5300 m a.m.s.l., we assume that melt refreezes before it reaches the glacier catchment outlet.

Estimation of the net radiation through remote sensing

The SEBAL inferences are carried out at the SRTM DEM resolution. The Rn in W m^{-2} is estimated using equation (3), where α is the dimensionless surface albedo, $R_L\downarrow$ is in W m^{-2}, and $R_L\uparrow$ in W m^{-2} is the outgoing longwave radiation. The ε_O is the dimensionless surface emissivity. The ε_O is 0.999 on snow surfaces (Morse *et al.*, 2000). For our analysis, ε_O is considered to be an uncertain parameter.

$$Rn = (1-\alpha)Rs + R_L\downarrow + R_L\uparrow - (1-\varepsilon_O)R_L\downarrow \tag{3}$$

The narrow band albedo (α_{TOA}) is transformed into α using equation (4) (Bastiaanssen, 2000), where ω is a dimensionless weighting coefficient, ρ is the dimensionless planetary reflectance at the top of the atmosphere, each Landsat band is denoted as Λ, α_p is the sun radiation reflected from the atmosphere, and τ_{SW} is the dimensionless atmospheric transmissivity of clear skies. The standardized mean solar exo-atmospheric spectral irradiance ESUN in W m^{-2} μm^{-1} is used to calculate ω (equation (5)) (Chander *et al.*, 2009). The α_p is assumed to be around 0.03 (Morse *et al.*, 2000). For our analysis, α_p is considered an uncertain parameter. The τ_{SW} is estimated with equation (6) (Bastiaanssen, 2000), where z is the SRTM DEM surface elevation in m a.m.s.l. Further uncertain topographic corrections are neglected (Riaño *et al.*, 2003).

$$\alpha = \left(\alpha_{TOA} - \alpha_p\right)\tau_{SW}^{-2} = \left[\Sigma(\omega_\Lambda \cdot \rho_\Lambda) - \alpha_p\right]\tau_{SW}^{-2} \tag{4}$$

$$\omega_\Lambda = \frac{\mathrm{ESUN}_\Lambda}{\Sigma(\mathrm{ESUN}_\Lambda)} \tag{5}$$

$$\tau_{SW} = 0.75 + 2 \cdot 10^{-5} \cdot z \tag{6}$$

Rs in W m^{-2} is estimated with equation (7) (Morse *et al.*, 2000), where the solar constant Gsc is 1367 W m^{-2}, $90-\beta$ is the sun elevation angle, d^2 is the Earth–sun distance in astronomical units:

$$Rs = Gsc(90-\beta)\tau_{SW} \cdot d^{-2} \tag{7}$$

The $R_L\uparrow$ and $R_L\downarrow$ in W m^{-2} are estimated with the Stefan-Boltzmann Law using equations (8) and (9), respectively (Morse *et al.*, 2000), where Ts (in K) is the surface temperature, Ta (in K) is the absolute air temperature at the reference height, and the Stefan-Boltzmann constant σ_{SB} is 5.67 10^{-8} W m^2 K^{-4}. The Ts is estimated from the brightness temperature detected by the sensors Tb and ε_o using equation (10) (Chander *et al.*, 2009), where K1 and K2 in W m^{-2} sr μm^{-1} are Landsat calibration constants, and L_Λ in W m^{-2} sr μm^{-1} is the spectral radiance at the sensor's aperture. The ε_{eff} is the non-dimensional effective atmospheric emissivity (about 0.7 on snow and ice covered surfaces, Morse *et al.*, 2000). For our analysis, ε_{eff} is considered an uncertain parameter.

$$R_L\uparrow = \varepsilon_o \sigma_{SB} Ts^4 \tag{8}$$

$$R_L\downarrow = \varepsilon_{eff} \sigma_{SB} Ta^4 \tag{9}$$

$$Ts = \frac{1}{\varepsilon_o^{0.25}} Tb = \frac{1}{\varepsilon_o^{0.25}} \cdot \frac{\mathrm{K2}}{\ln(\mathrm{K1}/L_\Lambda + 1)} \tag{10}$$

Ta may be approximately equal to Ts on areas where most of the energy is spent on sublimation (e.g. Morse *et al.*, 2000). For our analysis in winter season, the latter mentioned assumption may be erroneous, because of which the spatial distribution of the Ta is inferred under the assumption that the temperature gradient between Ts and Ta at the observation site is constant along the entire surface of the glacier.

Uncertainty analysis, numerical experiments, and uncertain model parameters

Variance-based techniques have the advantage for interpreting the uncertainty contributions of mutual parameter interactions to the total output variance. In summary, the technique estimates the contributed variance of u model parameters (each denoted by sub indices i,j….k) to model output $Y = f(u_i, u_j, .., u_k)$. After theoretically decomposing the total variance of the model output $V(Y)$ into summands of decreasing dimensions, sensitivity indices measure the relevance of the parameter contribution to total variance (Chan *et al.*, 2000). Each term on the decomposition is computable by Monte Carlo integrations (see Chan *et al.*, 2000). In this analysis, the interpretation of the numerical experiments is carried through the total order index S_{Ti} at every grid cell. The S_{Ti} denotes the main effect of parameter u_i, as well as its interactions, and it is interpreted as the expected percentage of variance that remains if all parameters were known but u_i (Chan *et al.*, 2000). As an importance measure, S_{Ti} evaluates the importance of a parameter as the percentage of the output variance associated with it (Chan *et al.*, 2000). Equation (11) calculates the S_{Ti}, where V_{-i} denotes the influence on the variance of all the factors except u_i. For details on applications, the reader is referred to Tang *et al.* (2007) and Soria & Kazama (2011):

$$S_{Ti} = (1 - V_{-i}) \cdot [V(Y)]^{-1} \tag{11}$$

For our analysis we carried out 1024 experiments with a sample size of 128. The uncertain parameters are those that could be calibrated. Three model parameters were tested in the sensitivity analysis of the net radiation equation: αp on behalf of the α and Rs component, ε_O on behalf of the $RL\uparrow$ component, and ε_{eff} on behalf of the RL↓ component. The uncertainty bounds assumed for each uncertain parameter are the same for each grid cell. Table 1 summarizes the uncertain parameters and the corresponding uncertainty bounds. The Sobol quasi-random sequence for non-correlated parameters is used to generate the sample (Chan *et al.*, 2000), 1024 values of M are calculated, and the set of M values is interpreted through the S_{Ti} calculated for each grid cell.

Table 1 Uncertainty range for the model parameters.

Model component	Model parameter	Uncertainty range
α	α_{TOA}	None (non-calibratable parameter)
	ω_Λ	None (non-calibratable parameter)
	α_p	0.025 to 0.040 (calibratable parameter)
	z	None (non-calibratable parameter)
	τ_{SW}	None (non-calibratable parameter)
Rs	Gsc	None (non-calibratable parameter)
	$90 - \beta$	None (non-calibratable parameter)
	d^2	None (non-calibratable parameter)
$R_L\uparrow$	σ_{SB}	None (non-calibratable parameter)
	ε_O	0.900 to 0.999 (calibratable parameter)
Ts	Tb	None (non-calibratable parameter)
	K1 and K2	None (non-calibratable parameter)
	L_Λ	None (non-calibratable parameter)
	Ts	Function of ε_O
$R_L\downarrow$	ε_{eff}	0.6 to 1.0 (calibratable parameter)
	Ta	None (non-calibratable parameter)

α: surface albedo; α_{TOA}: albedo at the top of the atmosphere; ω_Λ: weighting coefficient for α_{TOA}; α_p: sun radiation reflected from the atmosphere; z: surface elevation; τ_{SW}: atmospheric transmissivity; Rs: incoming shortwave radiation; Gsc: solar constant; $90 - \beta$: sun elevation angle; d^2: Earth–sun distance; $R_L\uparrow$: outgoing longwave radiation; σ_{SB}: Stefan-Boltzmann constant; ε_O: surface emissivity; Ts: surface temperature; Tb: at-sensor brightness temperature; K1, K2: calibration constants; L_Λ: spectral radiance at the sensor's aperture; $R_L\downarrow$: incoming longwave radiation; ε_{eff}: effective atmospheric emissivity; Ta: absolute air temperature.

RESULTS

The uncertainty analysis summarized in Fig. 1 compares the S_{Ti}s calculated for ε_O and ε_{eff} and the α values. Changes in α_p show a very low sensitivity on the α component, because of which the corresponding results are not presented in Fig. 1. The sensitivity of ε_{eff} is higher compared to the sensitivity of the other two model parameters tested, which not only suggests the dominance of the $R_L\downarrow$ on the sensitivity of the net radiation calculations over the Zongo glacier during the winter season, but interestingly reveals the high predictive uncertainty expected on melt estimates over the ablation area around the region where the monitoring station is installed (marked as a white circle on the central region of the glacier in Fig. 1). However, the results show that in the region where the highest uncertainties in net radiation predictions are likely, low rates of specific melt discharge (SMD) should be expected because of the high surface albedo (the calculated SMD uncertainty range in the central zone of the ablation area is 72–88 L s^{-1} km^{-2}).

As the surface albedo decreases in the vicinity of the lateral moraines and the glacier terminus, it also decreases the predictive uncertainty of the net radiation, as well as the sensitivity of the net radiation component terms. Simultaneously, as the surface albedo values decrease, the rates of predicted SMD increase considerably; in consequence, it increases the relevance of a predictive uncertainty that is apparently smaller than the predictive uncertainty observed in the glacier zone with high surface albedo (the calculated SMD uncertainty range on the boundaries of the glacier is in the range 128–143 L s^{-1} km^{-2}).

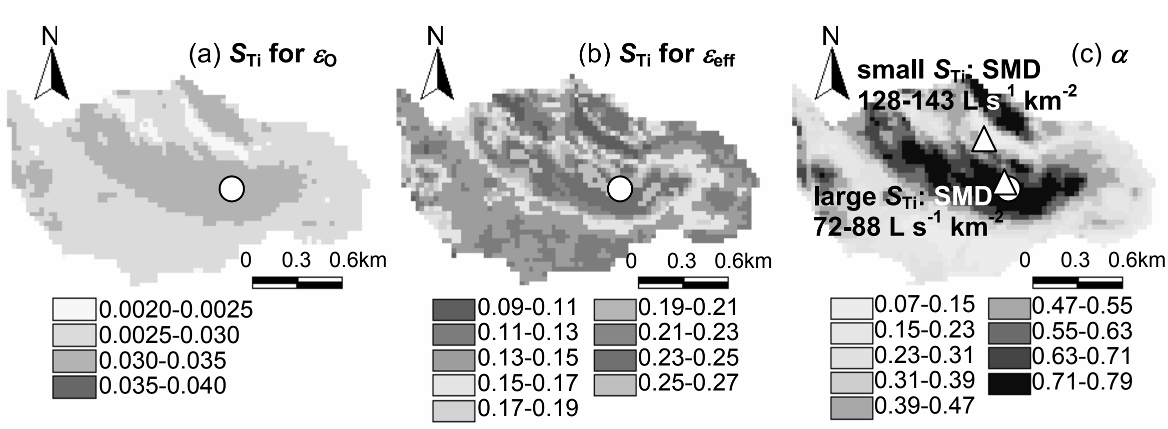

Fig. 1 Spatial distribution of the dimensionless total order index S_{Ti} on the Zongo glacier calculated for 26 July 2006 (10:30 h, local time). The figures correspond to the: (a) surface emissivity ε_O; (b) effective atmospheric emissivity ε_{eff}; and (c) spatial distribution of the surface albedo α for the Monte Carlo run with the highest calculated values. The white circles indicate the approximate location of the monitoring station; white triangles indicate the pixels where the smallest (small S_{Ti}) and the largest uncertainties (large S_{Ti}) are expected. Also shown are the ranges of specific melt discharge values (SMD) in L s^{-1} km^{-2} calculated on the latter mentioned locations.

In the melt season, the coincidence with the accumulation season should cause the glacier surface area having high albedo to grow; in consequence, the areal extent of the glacier where high melt predictive uncertainties are expected should also increase. However, considering that the melt rates on the region with high albedo are likely to be lower than the melt rates on the glacier boundaries, the overall uncertainty in melt predictions during the melt season should be expected to be smaller than the overall uncertainty expected in melt predictions during the dry-winter season over the glacier caps of the Cordillera Real.

CONCLUSIONS

The dominance of the albedo on the estimation of the spatial distribution of the net radiation is a known fact that has been demonstrated throughout our results. From the perspective of the net radiation investigation, the highest net radiation predictive uncertainties should be expected in glacier areal portions with higher surface albedo. Conversely, the numerical experiments described reveal that, when the aim is the calculation of glacier melt, a high predictive uncertainty should be expected over the glacier portions with low surface albedo, because those areal portions determine the areas with higher melt potential. For glacier melt estimations on the central part of the glacier with high surface albedo, the high predictive uncertainty may be attenuated by the low potential discharge associated with a high surface albedo. The conclusions also apply for assessing the installation of a monitoring network, because a more dense measuring network would be desired on the glacier areal portions that drive higher uncertainties in the predictions.

Acknowledgements The research was carried out by GRANDE project, supported by JST/JICA, SATREPS (Science and Technology Research Partnership for Sustainable Development), Japan. The meteorological data were provided by the French SO/ORE network GLACIOCLIM supported by IRD, the French Research Ministry, and local partners (IHH in Bolivia).

REFERENCES

Bastiaanssen, W. (2000) SEBAL-based sensible and latent heat fluxes in the irrigated Gediz Basin, Turkey. *J. Hydrol.* **229**, 87–100.

Beven, K. (1993) Prophecy, reality and uncertainty in distributed hydrological modelling. *Adv. Water Resour.* **16**, 41–51.

Chan, K., Tarantola, S., Saltelli, A. & Sobol, I. (2000) Variance-based methods. In: *Sensitivity Analysis* (ed. by A. Saltelli, K. Chan & E. Scott), 174–195. John Wiley, Chichester, UK.

Chander, G., Markhamb, B. & Dennis, H. (2009) Summary of current radiometric calibration coefficients for Landsat MSS, TM, ETM+, and EO-1 ALI sensors. *Remote Sens. Environ.* **113**(5), 893–903.

Morse, A., Allen, R., Tasumi, M., Kramber, W., Trezza, R. & Wright, J. (2000) Application of the SEBAL Methodology for estimating consumptive use of water and streamflow depletion. *Idaho Department of Water Resources – Final Report.*

Paterson, W. (1994) *The Physics of Glaciers*. Elsevier Science, Oxford, UK.

Riaño, D., Chuvieco, E., Salas, J. & Aguado, I. (2003) Assessment of different topographic corrections in Landsat TM data for mapping vegetation types. *IEEE Trans. Geosci. and Remote Sens.* **41**(5), 1056–1061.

Rick, U. (2008) Meltwater transport through firn in the accumulation zone of the Greenland ice sheet. PhD Thesis (abstract), University of Colorado, USA.

Sicart, J., Ribstein, P., Francou, B., Pouyaud, B. & Condom, T. (2007) Glacier mass balance of tropical Zongo glacier, Bolivia, comparing hydrological and glaciological methods. *Global and Planet. Change* **59**, 27–36.

Sicart, J., Hock, R. & Six, D. (2008) Glacier melt, air temperature, and energy balance in different climates: the Bolivian Tropics, the French Alps, and northern Sweden. *J. Geophys. Res.* **113**, D24113.

Soria, F. & Kazama, S. (2009) Evaluation of climate change effects on glacier area and vegetation using remote sensing imagery. *Proc. 7th Int. Symp. on Ecohydraulics ISE & 8th Hydroinformatics Int. Conf.*, Concepcion, Chile.

Soria, F. & Kazama, S. (2010) Potential impacts of climate change on the tropical Andes. *Annual J. Hydraul. Engng. JSCE.* (submitted).

Soria, F. & Kazama, S. (2011) Assessing streamflow source areas investigation through uncertainty evaluation of numerical experiments in small catchments. *Hydrol. Processes* (accepted).

Tang, Y., Reed, P., van Werkhoven, K. & Wagener, T. (2007) Advancing the identification and evaluation of distributed rainfall–runoff models using global sensitivity analysis. *Water Resour. Res.* **43,** W06415.

Wagener, T., Wheater, H. & Gupta, H. (2004) *Rainfall–Runoff Modelling in Gauged and Ungauged Catchments*. Imperial College Press, London, UK.

Wagnon, P., Ribstein, P., Kaser, G. & Berton, P. (1999) Energy balance and runoff seasonality of a Bolivian glacier. *Global and Planet. Change* **22**, 49–58.